ACS Energy Letters

http://pubs.acs.org/journal/aelccp

Solar Energy Storage by a Heterostructured $BiVO_4$–PbO_x Photocapacitive Device

Saeid Safshekan,[†,‡] Isaac Herraiz-Cardona,[†] Drialys Cardenas-Morcoso,[†] Reza Ojani,[‡] Marta Haro,[†] and Sixto Gimenez*,[†]

[†]Institute of Advanced Materials (INAM), Universitat Jaume I, 12006 Castelló, Spain

[‡]Electroanalytical Chemistry Research Laboratory, Faculty of Chemistry, University of Mazandaran, Babolsar, Iran

Supporting Information

ABSTRACT: The development of solar energy storage strategies is a key step for handling the inherent variability of sunlight within a global solar-based energy model. In the present study, we have developed a photocapacitive device based on the heterostructured $BiVO_4$–PbO_x system. $BiVO_4$ provides the photoactive core of the device, while PbO_x nanoparticles (formed by the controlled oxidation of colloidal PbS quantum dots) furnish a capacitive platform by redox pseudocapacitance. The synergistic coupling of these two systems leads to high capacitance under illumination, which can be subsequently released in the dark. This integrated device exhibits excellent behavior in terms of solar light harvesting (band gap in the visible region ~2.4 eV), with a specific capacitance of 6 mF cm^{-2} (4.5 mF cm^{-2} at discharge current density of 0.015 mA cm^{-2}), high open-circuit potential (1.5 V vs RHE), and stable charge–discharge cycling during 100 cycles, opening promising research avenues in the development of novel solar energy conversion–storage strategies.

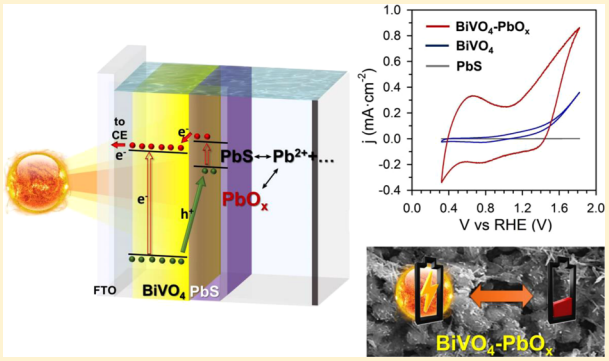

The development of energy schemes in which solar radiation acts as the energy input constitutes the only viable alternative to meet the near-future global demand in a sustainable fashion. The most advanced solar-to-electricity (photovoltaic) schemes available have demonstrated remarkable conversion efficiencies up to 46% and are steadily increasing year by year.[1] However, photovoltaic technologies are limited by the inherent daily and seasonal variability of solar radiation, and reliable energy storage strategies are required to shape a robust and secure solar-based global energy model. In this context, artificial photosynthesis to produce solar fuels (H_2 from water splitting or complex hydrocarbons from CO_2 reduction) constitutes an attractive solution to store solar energy in the chemical bonds of added-value chemicals, which can be stored, transported, and used upon demand.[2] Batteries are also at the forefront of mainstream research in energy storage and are steadily increasing their commercial application range from microchips to passenger vehicles.[3,4] Coupling electrical storage devices to renewable sources like sunlight provides a smart solution to store solar energy in an integrated device with potential application in several domains.[5−16]

In the past decade, some interesting approaches have been reported to harvest solar radiation with photocapacitive devices, which is a novel paradigm of energy conversion and storage. In the general scheme, solar radiation charges the photocapacitor and the discharge process takes place in the dark. The first devices were based on photovoltaic cells coupled to capacitive layers (i.e., dye-sensitized semiconductor, hole-trapping layer, and activated carbon particles in contact with an organic electrolyte solution).[17,18] The high complexity of this device configuration inherently brings cost and reliability issues, which can be partially overcome by integrating both functionalities in a single (capacitive) photoelectrode. As a remarkable example, Xia et al. developed photocapacitive electrodes based on TiO_2/nickel hydroxides core–shell nanorods.[19] The photogenerated holes at TiO_2 are stored by the chemical conversion of $Ni(OH)_2$ to NiOOH, and the corresponding reductive energy (photoelectrons) can be directly utilized for H_2 evolution. A multifunctional system based on TiO_2 nanowire/NiO nanoflakes photoanode and Si nanowire/Pt nanoparticle photocathode has been reported for simultaneous solar energy conversion, energy storage, and chemical sensing.[20] However, the high band gap of TiO_2 (~3.2 eV) and the low charge–discharge stability of $Ni(OH)_2$/NiOOH constitute the main drawbacks of these systems. Therefore, further alternatives need to be explored, particularly on lower band gap semiconductors,

Received: December 24, 2016
Accepted: January 23, 2017

DOI: 10.1021/acsenergylett.6b00728
ACS Energy Lett. 2017, 2, 469−475

in order to more efficiently harvest solar radiation with competitive stability.

The "defect tolerant" n-type bismuth vanadate, $BiVO_4$, with monoclinic (scheelite-type) structure has been identified as a promising photoanode material for different photoelectrochemical applications like water oxidation[21,22] photocatalysis and degradation of pollutants.[21,22] This material can be excited under visible light irradiation (band gap, ~2.4 eV). The electronic properties of this material are hampered by high bulk recombination losses.[23,24] Consequently, different strategies like gradient doping,[25] photocharging,[26] or heterostructuring with larger band gap semiconductors[27−30] have been developed to notably improve the photoelectrochemical performance of this material, circumventing its poor bulk properties. In the present study, $BiVO_4$ material is employed as the photoactive core of a novel photocapacitive system, absorbing solar radiation to generate electrons and holes. The photogenerated holes are subsequently stored in a capacitive PbO_x top layer. This storage platform is obtained through controlled photo-oxidation of PbS quantum dots. The combination of both materials provides a singular heterostructured system ($BiVO_4$−PbO_x) capable of converting and storing solar energy within an intrinsically single structure with outstanding stability toward charge−discharge cycling and fast charge rate without applying any electrical bias under only solar illumination.

PbS QDs and uniform film of $BiVO_4$ were prepared, with some modifications, according to methods previously reported in the literature.[31,32] The as-synthesized $BiVO_4$−PbS heterostructures were conditioned by cyclic voltammetry in a phosphate buffer solution (pH ≈ 7) with a sequence of 100 scans between 0.3 and 1.8 V vs RHE (Figure 1a), where the controlled oxidation of PbS to PbO_x takes place. During the first scan, the pristine $BiVO_4$−PbS photoelectrode shows an anodic response, which can be related to the first oxidation step of PbS with low capacitance. As the number of scans increases, the system exhibits enhanced capacitive behavior, as shown by the hysteretic enlargement of the cyclic voltammetry scans. Indeed, after 40 scans, the pseudocapacitive shape of the cyclic voltammograms is already defined, and further changes are not observed during the subsequent cycles. After 100 scans, because of the complete oxidation of PbS, a stable voltamogram showing high capacity is observed (determined by the width of the anodic and cathodic sweep). In contrast, no photocapacitive response was obtained when the individual components ($BiVO_4$ and PbS) were tested in the same conditions (see Figure S1 in the Supporting Information), clearly suggesting a synergistic interaction between $BiVO_4$ and the oxidized product of PbS (PbO_x) for the observed photocapacitive behavior. In the dark, the conditioned $BiVO_4$−PbO_x heterostructure does not retain any capacitance, as shown in Figure 1b, indicating that the capacitive behavior is related to the photogenerated charges at the $BiVO_4$ electrode under illumination. In this figure, the footprint-specific photocapacitance of the $BiVO_4$−PbO_x heterostructure was measured as ~6 mF cm^{-2} according to the expression

$$C = [(I_a + I_c)/2]/dV\,dt^{-1} \quad (1)$$

where I_a and I_c are related to the anodic and cathodic peak photocurrents. This value of ~6 mF cm^{-2} nicely matches that obtained by impedance spectroscopy (IS), as shown in the Bode plot of the capacitance (real part of the capacitance vs frequency) in Figure 1c, of about 7 mF cm^{-2} in the low-frequency region. The presence of a second plateau in the Bode

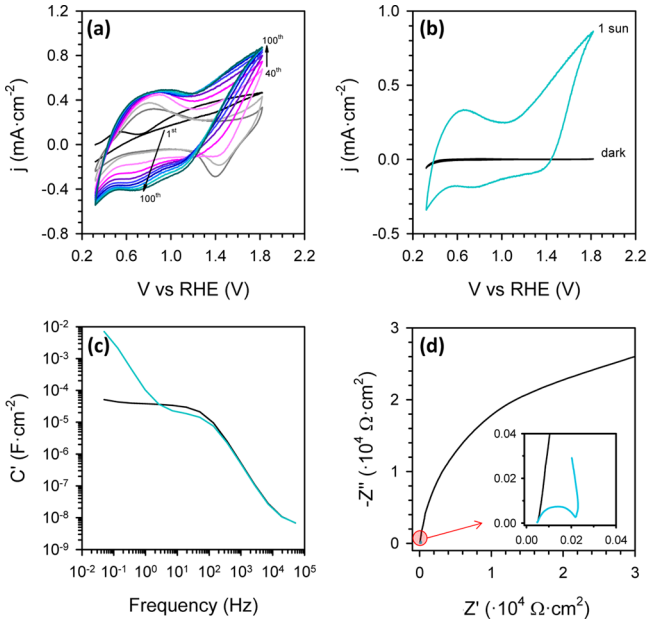

Figure 1. (a) Successive cyclic voltammetry scans between 0.3 and 1.9 V vs RHE at 100 mV s^{-1} (100 cycles) under illumination at 100 mW cm^{-2} in phosphate buffer solution (pH ≈ 7) for the $BiVO_4$−PbS heterostructure. (b) Response of the $BiVO_4$−PbO_x photocapacitor in the dark and under illumination at 50 mV s^{-1}. (c) Real part of the capacitance (C') versus frequency (Bode plot) in the dark and under illumination. (d) Nyquist plot ($-Z''$ vs Z') obtained from impedance measurements for the photocapacitor in the dark and under illumination obtained at a constant potential of 0.62 V vs RHE.

representation also supports the idea of a chemical capacitance under illumination, while the electrochemical double-layer (EDL) capacitance is observed at 10−100 Hz with the typical value of ca. 10^{-5} F cm^{-2}.[33] In the dark, this EDL capacitance corresponds to the only plateau observed in Figure 1c with a value around 8×10^{-5} F cm^{-2}. Figure 1d shows the Nyquist plots ($-Z''$ vs Z') in the dark and under illumination. A high resistance of the $BiVO_4$−PbO_x system is observed in the dark, while it is reduced to ca. 200 Ω cm^2 under illumination. This resistance is in parallel to the EDL capacitance and it is ascribed to the charge-transfer resistance, indicating the appearance of faradaic phenomena. The charge transfer in the system under illumination produces a high increase of the capacitance (imaginary part of the Nyquist plot), providing evidence that the charge is stored in the $BiVO_4$−PbO_x electrode.

In order to evaluate when water oxidation (oxygen evolution reaction, OER) competes with the accumulation of holes within the PbO_x layer, chronoamperometric and impedance spectroscopy measurements were carried out at different applied voltages under illumination (Figure S2). At voltages higher than 1.6 V vs RHE, the low-frequency impedance starts to evolve from a purely capacitive behavior (vertical line) to a resistive one (semicircle), indicating the appearance of faradaic phenomena. At higher voltages, the faradaic phenomena are more important, and at 2 V vs RHE, a second arc at low frequency is observed, indicating a low charge-transfer resistance. From this potential on, the dominant phenomenon is OER. This behavior is consistent with chronoamperometric measurements. Applied voltages higher than 1.5 V vs RHE lead to a steady-state photocurrent, which increases with voltage. Conversely, identical cathodic response is systematically

DOI: 10.1021/acsenergylett.6b00728
ACS Energy Lett. 2017, 2, 469−475

obtained, supporting the idea that the steady-state photocurrent is related to the OER process.

The (photo)electrochemical behavior of the $BiVO_4$−PbO_x photocapacitors was also characterized by cyclic voltammetry for different scan rates. In the dark (Figure S3a), very small anodic and cathodic currents were obtained with a well-defined redox peak. The peak current is first-order with scan rate as shown by the inset of Figure S3a, indicating a surface-confined redox process, and consequently it was assigned to the V^{4+}/V^{5+}redox couple.[34,35] On the other hand, the high anodic and cathodic currents under illumination increasing with scan rate (Figure S3b) are consistent with the photocapacitive behavior shown in Figure 1a.

To understand the origin of this synergistic photocapacitive behavior, a detailed structural and surface characterization was carried out. The morphology of different electrodes was investigated with scanning electron microscopy (SEM). The structure of the $BiVO_4$ film (Figure S4), shows some submicrometric pores and cavities between the particles, reducing the pathway of photogenerated holes to reach the surface of $BiVO_4$, in good agreement with previous studies.[32] Upon spin coating PbS quantum dots, the surface of $BiVO_4$ particles was covered with a layer of oleic acid capped PbS, as described in the Supporting Information and illustrated in Figure 2a. Transmission electron microscopy (TEM) examination of the pristine $BiVO_4$−PbS photoelectrodes shows the presence of a nearly monodispersed distribution of spherical nanoparticles with diameter around 3 nm (Figure 2c). The chemical composition of these nanoparticles evaluated by both Energy Dispersive Spectroscopy (EDS) and X-ray Photoelectron Spectroscopy (XPS) agrees well with that of PbS (see below). The arrow in Figure 2c shows a crystalline nanoparticle with interplanar distance of 3 Å, which corresponds to the (200) planes of rock salt PbS. After 100 cyclic voltammetry scans under illumination in phosphate buffer, the development of needle-like features related to the PbO_x species produced by the controlled oxidation treatment can be seen from the top view in Figure 2b and the TEM images in Figure 2d. After the controlled oxidation process by cyclic voltammetry in phosphate buffer, the spherical PbS quantum dots are not detected, and larger features with characteristic dimension >10 nm are present, which suggest the transformation of PbS into PbO_x. One of the arrows in Figure 2d shows a 15 nm diameter nanocrystal with interplanar distance of 2.60 Å, which corresponds to the (111) planes of orthorhombic PbO_2. Most of the identified nanoparticles showed this interplanar distance, although few particles (see Figure 2d) exhibited an interplanar distance of 2.38 Å, which corresponds to the (201) planes of orthorhombic PbO. Magnified views of Figure 2c,d are included in Figure S5, in which the lattice fringes can be visualized together with the graphical process for the determination of the lattice spacing. These PbO_x nanoparticles appear embedded in needle-shaped structures, and the energy-dispersive spectrometry analysis from SEM measurements shows the presence of Pb and O, as shown in Figure S6. The assignment carried out by TEM is further corroborated by XPS experiments. Figure 3a shows the XPS spectra corresponding to the S 2s signal from $BiVO_4$−PbS surface before and after the controlled oxidation process by cyclic voltammetry. In the pristine electrode, this signal appears at binding energy of 225.1 eV, agreeing well with the presence of PbS. After the controlled oxidation process, this peak is no longer visible, indicating that sulfur is totally depleted from the surface. On the other hand, the intensity of the O KLL Auger peak (Figure 3b) is significantly increased after cyclic voltammetry, clearly suggesting the increase of O at the surface, as PbO or PbO_2. Finally, the Pb $4f_{7/2}$ signal for both pristine and treated specimens is shown as Figure 3c. The interval of binding energies for the Pb $4f_{7/2}$ signal when Pb is present as PbO is 137.6−138.2 eV. On the other hand, when Pb is present as PbO_2, the binding energy for the Pb $4f_{7/2}$ signal is 136.8−138.2 eV. Consequently, both compounds would be possible from our analyses. In any case, both TEM and XPS provide clear evidence for the transformation of PbS into PbO_x. Because both PbO_2 and PbO phases were identified in the oxidized specimens, we will refer to PbO_x (where x = 1, 3/2, 2), although the major contribution in the analyzed specimens comes from PbO_2. The presence of interfacial trap states at the $BiVO_4$/PbX interface cannot be ruled out. Further insights into this issue would require the use of experimental techniques such as admittance spectroscopy as well as deep level spectroscopy[36] or theoretical tools as density functional theory calculations[37] to provide a detailed mapping of the electronic states at the $BiVO_4$/PbX interface.

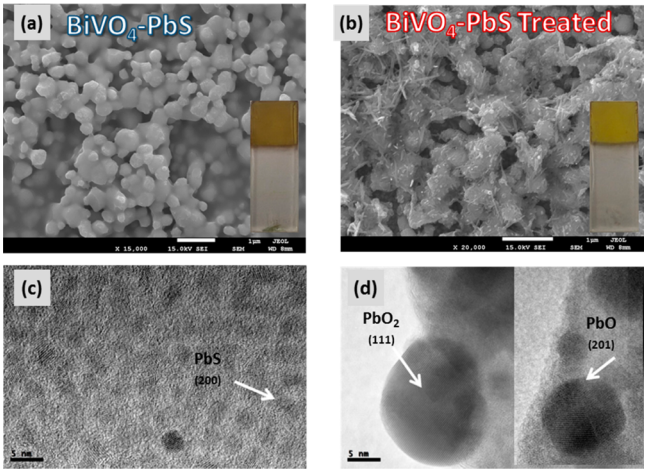

Figure 2. SEM images of $BiVO_4$−PbS before (a) and after (b) cyclic voltammetry in phosphate buffer. TEM images of the $BiVO_4$−PbS system before (c) and after (d) undergoing cyclic voltammetry in phosphate buffer. The arrow in panel c shows a PbS quantum dot, 3 nm diameter with interplanar distance of 3 Å, which corresponds to the (200) planes of PbS. The arrows in panel d show nanocrystals with interplanar distance of 2.60 Å, which corresponds to the (111) planes of orthorhombic PbO_2, and a nanocrystal with interplanar distance of 2.38 Å, which corresponds to the (201) planes of orthorhombic PbO.

At this point, it is important to highlight the importance of the preparation method for the obtained $BiVO_4$−PbO_x structures. The electrochemical oxidation of the PbS precursor provides a gradual and controlled evolution of PbS to PbO_x. On the other hand, alternative methods like thermal oxidation were also tested (details are provided in Figure S7), leading to a different morphology and structure of the obtained material, with no photocapacitive behavior. This suggests that electrochemical oxidation is the optimum route for the preparation of the photocapacitive $BiVO_4$−PbO_x system.

On the other hand, the optical properties of the $BiVO_4$−PbS heterostructure were also evaluated by ultraviolet−visible spectrophotometry (Figure S8). The excellent light-harvesting capabilities of the photocapacitor can be inferred from an

DOI: 10.1021/acsenergylett.6b00728
ACS Energy Lett. 2017, 2, 469−475

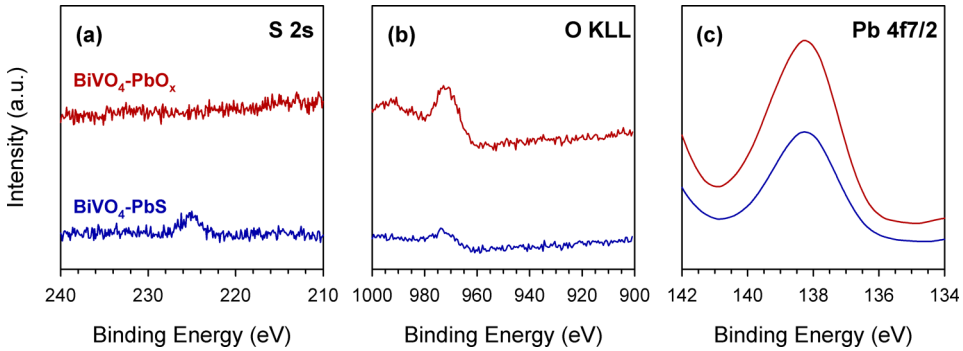

Figure 3. (a) S 2s, (b) O KLL, and (c) Pb $4f_{7/2}$ levels extracted from XPS for $BiVO_4$−PbS heterostructures before and after 100 cyclic voltammetry scans.

enhancement in absorbance below 500 nm, which is consistent with the transformation of PbS into PbO_x.[38,39]

In summary, SEM, TEM, and XPS demonstrate that after 100 cycles the species formed on top of the $BiVO_4$ electrode is PbO_x, while no trace of S is detected in the electrode. Consequently, the suggested mechanism for the formation of the $BiVO_4$−PbO_x heterostructure is illustrated in Figure 4a.

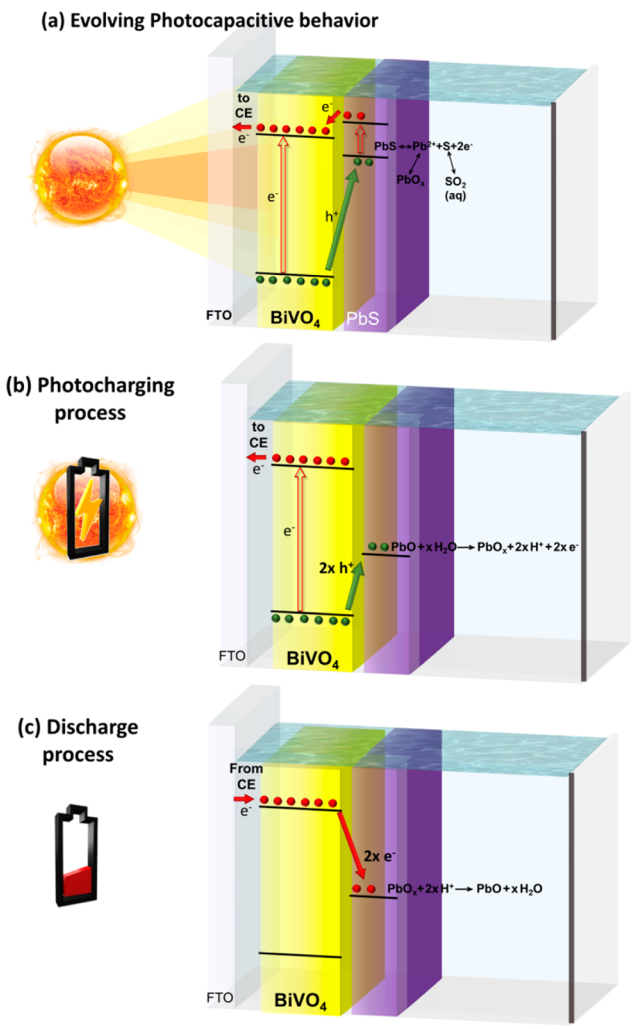

Figure 4. (a) Proposed mechanism for the evolution of $BiVO_4$−PbO_x photocapacitor system and both (b) photocharge and (c) discharge processes.

Under illumination, the photgenerated carriers at the $BiVO_4$ layer are separated (reaction 2) because of the electric field developed at the heterojunction.

$$BiVO_4 + h\nu \rightarrow BiVO_4 + h^+ + e^- \quad (2)$$

Then, photo-oxidation of the PbS quantum dots into Pb^{2+} and S takes place:

$$PbS + 2h^+ \leftrightarrow Pb^{+2} + S \quad (3)$$

This reaction occurs at ca. 0.35 V vs RHE,[40−42] where the oxidation peak during the first CV scan is observed.

Once S is formed, the dissolution and oxidation to SO_2(aq) at the same voltage takes place, consistent with the absence of detected S by any of the experimental techniques used. On the other hand, Pb^{2+} can be subsequenltly photo-oxidized to PbO_x at the $BiVO_4$ surface as evidenced by TEM and XPS and consistent with a recent report.[43] Some authors have also reported the formation of $PbBiVO_5$[44] at high temperatures. In this case, XRD measurements (Figure S9) clearly indicate that this phase is not formed, in good agreement with the formation of a $BiVO_4$−PbO_x interfacial layer. The persistence of the monoclinic $BiVO_4$ crystalline structure after partial reduction during photocharging is consistent with previous reported studies.[35]

Photocapacitive Mechanism. The photocapacitive device is based on the $BiVO_4$−PbO_x system, while SO_2 (aq) species are present in the electrolyte. To rule out that the possible capacitive mechanism was related to the redox chemistry of sulfide species, $BiVO_4$ was cycled in two different polysulfide redox solutions. The results (Figure S10) clearly show no photocapacitive response, demonstrating that the polysulfide chemistry does not control the capacitive response. Consequently, the photocapacitive mechanism is entirely ascribed to the $BiVO_4$−PbO_x heterostructure.

However, it is worth noting that the chemistry of lead (hydr)oxides is a subject of considerable complexity, and it can evolve in several mono- and polynuclear species.[45] Hence, we propose the following simplified reactions to show the evolution of the photocapacitive mechanism and the subsequent charge and discharge processes.

$$Pb^{+2} + H_2O \leftrightarrow PbO + 2H^+ \quad (4)$$

$$PbO + xH_2O + 2xh^+ \leftrightarrow PbO_x + 2xH^+ \quad (x = 1.5, 2) \quad (5)$$

This proposed mechanism is fully consistent with our results from TEM and XPS characterization. Futhermore, at

DOI: 10.1021/acsenergylett.6b00728
ACS Energy Lett. 2017, 2, 469−475

intermediate CV scans (cycles 5−10), the peak at ca. 1.45 V can be ascribed to the reduction of PbO_2 to Pb^{2+}. As shown in Figure 1a, this peak is not visible after 40 cycles, because the stabilized voltamograms with photocapacitive behavior is believed to be related to the PbO_x/PbO redox couple. In fact, a photoassisted oxidation of PbO (reaction 5) during the forward scan and a reduction reaction during the reverse scan will lead to a typical capacitive behavior.

Accordingly, Figure 4 shows a schematic representation for the proposed mechanism.

To fully assess the photocapacitive behavior and the stability of the developed photocapacitor, different key parameters were evaluated, as shown in Figure 5. First, the open-circuit potential

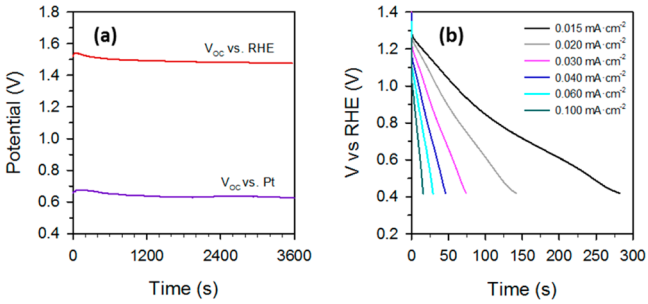

Figure 5. (a) Stability of open-circuit potential (OCV) of photocapacitor after charging for 30 s illumination under short-circuit conditions. In this plot, V_{oc} vs RHE refers to a three-electrode measurement, while V_{oc} vs Pt refers to a two-electrode measurement. (b) Galvanostatic discharge curves after a full charging of photocapacitor under light illumination for 30 s under short-circuit conditions.

of the fully charged photocapacitor was determined. For this purpose, the electrodes were illuminated at 100 mW cm^{-2} under short-circuit conditions (by wiring the $BiVO_4$−PbO_x electrode to the Pt counterelectrode) for 30 s. Subsequently, the cell was open-circuited to stop the electron flow, and the open-circuit potential (V_{OC}) of the fully charged photocapacitor was obtained using a three-electrode system in the dark. A remarkable value of V_{OC} around 1.5 V vs RHE was obtained (Figure 5a), significantly higher than that of other recently reported photocapacitors using TiO_2 and nickel.[12] This high V_{OC} is provided by the difference between the electron quasi-Fermi level (around 0 V vs RHE) and the hole quasi-Fermi level at the PbO_x interfacial layer electrode, because the reduction of PbO_2 takes place at 1.45 V vs RHE. Figure 5a also shows the high stability of the open-circuit voltage, which demonstrates the remarkably low current leakage of the photocapacitor after 1 h. It is worth noting that the device can also be electrochemically charged by applying high potentials to drive the electrochemical oxidation of lead oxide in the dark (Figure S11). On the other hand, the galvanostatic discharge curves after a full charging of the photocapacitor were obtained at a constant discharge current by monitoring the cell voltage as a function of time. The results for different currents normalized to the geometric surface area of the electrode, with the constant current densities from 0.015 to 0.1 mA cm^{-2}, are shown in Figure 5b. The capacitance of the system is 4.5 mF cm^{-2} at 0.015 mA cm^{-2}, a value close to the quasi-equilibrium stored energy calculated by impedance spectroscopy, but drops to 2.2 mF cm^{-2} at 0.1 mA cm^{-2}. The high novelty of this integrated system makes difficult the comparison with other reported photocapacitive systems. Compared to a recent system based on TiO_2 (1.1 mF cm^{-2} at 1 mA cm^{-2}),[6] the present system shows higher capacitance with the additional advantage of visible light absorption. Finally, we have evaluated its stability during cycling. Figure S12a shows the charge−discharge behavior. Here, the charge−discharge process was performed under on−off illumination cycles using an automatic chopped system, maintaining the system at 0.62 V vs RHE. At this voltage, no faradaic phenomena related to OER are competing with the accumulation of the holes at the PbO_x layer, and the measured current is purely related to the capacitive mechanism. As mentioned before, under illumination, photogenerated holes at $BiVO_4$ oxidize the synergistic storage system $BiVO_4$−PbO_x and an anodic current is recorded by the potentiostat. During this process, the surface of the photocapacitor is positively charged, and the initial photocharging current of 0.42 mA cm^{-2} exponentially decreases to near zero (fully charged photocapacitor). This behavior is similar to the charging behavior of standard capacitors under constant-voltage conditions. In the dark, the discharging process takes place, the electrons are driven from the oxidized $BiVO_4$−PbO_2 to their reduced form $BiVO_4$−PbO_x, and a reverse cathodic reaction takes place to neutralize the electrode. The charge stored and delivered by the system is of 1.35 mC cm^{-2}. As can be seen from Figure S12b, there is no apparent decrease of the storage ability of the system during 100 charge−discharge cycles, highlighting the outstanding stability of this heterostructured system.

In summary, we have developed a novel photocapacitive system based on the $BiVO_4$/PbS type II hetereostructure, which after controlled oxidation evolves to $BiVO_4$/PbO_x. The photocapacitive mechanism stems from the conversion of PbS into PbO_x as demonstrated by TEM and XPS measurements. To the best of the authors' knowledge, the photocapacitive behavior of this system outperforms the most advanced devices reported in the literature, showing a specific capacitance of 6 mF cm^{-2} (4.5 mF cm^{-2} at discharge current density of 0.015 mA cm^{-2}), high open-circuit potential (1.5 V vs RHE), and stable charge−discharge cycling during 100 cycles. Moreover, solar fuels in the form of H_2 gas could be generated during the charging step if the system is coupled to a water reduction photocathode. These results open promising research avenues in the development of novel solar energy conversion−storage strategies.

■ ASSOCIATED CONTENT

Supporting Information

The Supporting Information is available free of charge on the ACS Publications website at DOI: 10.1021/acsenergylett.6b00728.

Description of the materials and characterization methods employed and extensive information on the structural and photoelectrochemical characterization of the employed materials (PDF)

■ AUTHOR INFORMATION

Corresponding Author

*E-mail: sjulia@uji.es.

ORCID

Sixto Gimenez: 0000-0002-4522-3174

Notes

The authors declare no competing financial interest.

DOI: 10.1021/acsenergylett.6b00728
ACS Energy Lett. 2017, 2, 469−475

■ ACKNOWLEDGMENTS

We thank Generalitat Valenciana (ISIC/2012/008 Institute of Nanotechnologies for Clean Energies and ACOMP/2015/105) and the University Jaume I for financial support through the project P1·1B2011-50. We also gratefully acknowledge financial support of the Ministry of Science, Research and Technology (MSRT) of Iran, by means of scholarship grant for S.S. We also thank Dr. Mauricio Solis de la Fuente for the supply of PbS quantum dots. Prof. Juan Bisquert and Prof. Germà Garcia-Belmonte are acknowledged for fruitful discussions of this study.

■ REFERENCES

(1) Green, M. A.; Emery, K.; Hishikawa, Y.; Warta, W.; Dunlop, E. D. Solar Cell Efficiency Tables (version 48). *Prog. Photovoltaics* **2016**, *24*, 905−913.

(2) Walter, M. G.; Warren, E. L.; McKone, J. R.; Boettcher, S. W.; Mi, Q.; Santori, E. A.; Lewis, N. S. Solar Water Splitting Cells. *Chem. Rev.* **2010**, *110*, 6446−6473.

(3) Armand, M.; Tarascon, J. M. Building Better Batteries. *Nature* **2008**, *451*, 652−657.

(4) Winter, M.; Brodd, R. J. What Are Batteries, Fuel Cells, and Supercapacitors? *Chem. Rev.* **2004**, *104*, 4245−4269.

(5) Murakami, T. N.; Kawashima, N.; Miyasaka, T. A High-Voltage Dye-Sensitized Photocapacitor of a Three-Electrode System. *Chem. Commun.* **2005**, *26*, 3346−8.

(6) Xu, J.; Wu, H.; Lu, L.; Leung, S.-F.; Chen, D.; Chen, X.; Fan, Z.; Shen, G.; Li, D. Integrated Photo-Supercapacitor Based on Bi-Polar TiO_2 Nanotube Arrays with Selective One-Side Plasma-Assisted Hydrogenation. *Adv. Funct. Mater.* **2014**, *24*, 1840−1846.

(7) Cohn, A. P.; Erwin, W. R.; Share, K.; Oakes, L.; Westover, A. S.; Carter, R. E.; Bardhan, R.; Pint, C. L. All Silicon Electrode Photocapacitor for Integrated Energy Storage and Conversion. *Nano Lett.* **2015**, *15*, 2727−31.

(8) Ng, C. H.; Lim, H. N.; Hayase, S.; Harrison, I.; Pandikumar, A.; Huang, N. M. Potential Active Materials for Photo-Supercapacitor: A Review. *J. Power Sources* **2015**, *296*, 169−185.

(9) Hsu, C.-y.; Chen, H.-w.; Lee, K.-m.; Hu, C.-w.; Ho, K.-c A Dye-Sensitized Photo-Supercapacitor Based on PProDOT-Et_2 Thick Films. *J. Power Sources* **2010**, *195*, 6232−6238.

(10) Wee, G.; Salim, T.; Lam, M.; Mhaisalkar, G.; Srinivasan, M. Printable Photo-Supercapacitor Using Single-Walled Carbon Nanotubes. *Energy Environ. Sci.* **2011**, *4*, 413−416.

(11) Gong, M.; Kirkeminde, A.; Kumar, N.; Zhao, H.; Ren, S. Ionic-Passivated FeS_2 Photocapacitors for Energy Conversion and Storage. *Chem. Commun.* **2013**, *49*, 9260−2.

(12) Xia, X.; Luo, J.; Zeng, Z.; Guan, C.; Zhang, Y.; Tu, J.; Zhang, H. Integrated Photoelectrochemical Energy Storage: Solar Hydrogen Generation and Supercapacitor. *Sci. Rep.* **2012**, *2*, 981.

(13) Chen, T.; Qiu, L.; Yang, Z.; Cai, Z.; Ren, J.; Li, H.; Lin, H.; Sun, X.; Peng, H. An Integrated "Energy Wire" for Both Photoelectric Conversion and Energy Storage. *Angew. Chem., Int. Ed.* **2012**, *51*, 11977−11980.

(14) Zhang, Z.; Chen, X.; Chen, P.; Guan, G.; Qiu, L.; Lin, H.; Yang, Z.; Bai, W.; Luo, Y.; Peng, H. Integrated Polymer Solar Cell and Electrochemical Supercapacitor in a Flexible and Stable Fiber Format. *Adv. Mater.* **2014**, *26*, 466−470.

(15) Guo, W.; Xue, X.; Wang, S.; Lin, C.; Wang, Z. L. An Integrated Power Pack of Dye-Sensitized Solar Cell and Li Battery Based on Double-Sided TiO_2 Nanotube Arrays. *Nano Lett.* **2012**, *12*, 2520−2523.

(16) Shi, C.; Dong, H.; Zhu, R.; Li, H.; Sun, Y.; Xu, D.; Zhao, Q.; Yu, D. An "All-in-One" Mesh-Typed Integrated Energy Unit for Both Photoelectric Conversion and Energy Storage in Uniform Electrochemical System. *Nano Energy* **2015**, *13*, 670−678.

(17) Miyasaka, T.; Murakami, T. N. The Photocapacitor: An Efficient Self-Charging Capacitor for Direct Storage of Solar Energy. *Appl. Phys. Lett.* **2004**, *85*, 3932−3934.

(18) Murakami, T. N.; Kawashima, N.; Miyasaka, T. A High-Voltage Dye-Sensitized Photocapacitor of a Three-Electrode System. *Chem. Commun.* **2005**, 3346−3348.

(19) Xia, X.; Luo, J.; Zeng, Z.; Guan, C.; Zhang, Y.; Tu, J.; Zhang, H.; Fan, H. J. Integrated Photoelectrochemical Energy Storage: Solar Hydrogen Generation and Supercapacitor. *Sci. Rep.* **2012**, *2*, 981.

(20) Wang, Y.; Tang, J.; Peng, Z.; Wang, Y.; Jia, D.; Kong, B.; Elzatahry, A. A.; Zhao, D.; Zheng, G. Fully Solar-Powered Photoelectrochemical Conversion for Simultaneous Energy Storage and Chemical Sensing. *Nano Lett.* **2014**, *14*, 3668−3673.

(21) Kohtani, S.; Makino, S.; Kudo, A.; Tokumura, K.; Ishigaki, Y.; Matsunaga, T.; Nikaido, O.; Hayakawa, K.; Nakagaki, R. Photocatalytic Degradation of 4-N-Nonylphenol under Irradiation from Solar Simulator: Comparison between $BiVO_4$ and TiO_2 Photocatalysts. *Chem. Lett.* **2002**, *31*, 660−661.

(22) Yin, W. Z.; Wang, W. Z.; Shang, M.; Zhou, L.; Sun, S. M.; Wang, L. $BiVO_4$ Hollow Nanospheres: Anchoring Synthesis, Growth Mechanism, and Their Application in Photocatalysis. *Eur. J. Inorg. Chem.* **2009**, *2009*, 4379−4384.

(23) Shi, X.; Herraiz-Cardona, I.; Bertoluzzi, L.; Lopez-Varo, P.; Bisquert, J.; Park, J. H.; Gimenez, S. Understanding the Synergistic Effect of WO_3-$BiVO_4$ Heterostructures by Impedance Spectroscopy. *Phys. Chem. Chem. Phys.* **2016**, *18*, 9255−9261.

(24) Grigioni, I.; Stamplecoskie, K. G.; Selli, E.; Kamat, P. V. Dynamics of Photogenerated Charge Carriers in $WO_3/BiVO_4$ Heterojunction Photoanodes. *J. Phys. Chem. C* **2015**, *119*, 20792−20800.

(25) Abdi, F. F.; Han, L.; Smets, A. H. M.; Zeman, M.; Dam, B.; van de Krol, R. Efficient Solar Water Splitting by Enhanced Charge Separation in a Bismuth Vanadate-Silicon Tandem Photoelectrode. *Nat. Commun.* **2013**, *4*, 2195.

(26) Trzesniewski, B. J.; Smith, W. A. Photocharged $BiVO_4$ Photoanodes for Improved Solar Water Splitting. *J. Mater. Chem. A* **2016**, *4*, 2919−2926.

(27) Pihosh, Y.; Turkevych, I.; Mawatari, K.; Uemura, J.; Kazoe, Y.; Kosar, S.; Makita, K.; Sugaya, T.; Matsui, T.; Fujita, D.; et al. Photocatalytic Generation of Hydrogen by Core-Shell $WO_3/BiVO_4$ Nanorods with Ultimate Water Splitting Efficiency. *Sci. Rep.* **2015**, *5*, 11141.

(28) Rao, P. M.; Cai, L.; Liu, C.; Cho, I. S.; Lee, C. H.; Weisse, J. M.; Yang, P.; Zheng, X. Simultaneously Efficient Light Absorption and Charge Separation in $WO_3/BiVO_4$ Core/Shell Nanowire Photoanode for Photoelectrochemical Water Oxidation. *Nano Lett.* **2014**, *14*, 1099−1105.

(29) Shi, X.; Choi, Y.; Zhang, K.; Kwon, J.; Kim, D. Y.; Lee, J. K.; Oh, S. H.; Kim, J. K.; Park, J. H. Efficient Photoelectrochemical Hydrogen Production from Bismuth Vanadate-Decorated Tungsten Trioxide Helix Nanostructures. *Nat. Commun.* **2014**, *5*, 4775.

(30) Shi, X.; Zhang, K.; Shin, K.; Ma, M.; Kwon, J.; Choi, I. T.; Kim, J. K.; Kim, H. K.; Wang, D. H.; Park, J. H. Unassisted Photoelectrochemical Water Splitting Beyond 5.7%Solar-to-Hydrogen Conversion Efficiency by a Wireless Monolithic Photoanode/Dye-Sensitised Solar Cell Tandem Device. *Nano Energy* **2015**, *13*, 182−191.

(31) Sanchez, R. S.; Binetti, E.; Torre, J. a.; Garcia-Belmonte, G.; Striccoli, M.; Mora-Sero, I. All Solution Processed Low Turn-on Voltage near Infrared Leds Based on Core-Shell PbS-CdS Quantum Dots with Inverted Device Structure. *Nanoscale* **2014**, *6*, 8551−5.

(32) Kang, D.; Park, Y.; Hill, J. C.; Choi, K.-S. Preparation of Bi-Based Ternary Oxide Photoanodes $BiVO_4$, Bi_2WO_6, and $Bi_2Mo_3O_{12}$ Using Dendritic Bi Metal Electrodes. *J. Phys. Chem. Lett.* **2014**, *5*, 2994−2999.

(33) Bisquert, J. *Nanostructured Energy Devices. Equilibrium Concepts and Kinetics*; CRC Press, Taylor & Francis Group: Boca Raton, FL, 2015.

DOI: 10.1021/acsenergylett.6b00728
ACS Energy Lett. 2017, 2, 469−475

(34) Qin, D.-D.; Wang, T.; Song, Y.-M.; Tao, C.-L. Reduced Monoclinic $BiVO_4$ for Improved Photoelectrochemical Oxidation of Water under Visible Light. *Dalton Trans.* **2014**, *43*, 7691−4.
(35) Trześniewski, B. J.; Smith, W. A. Photocharged $BiVO_4$ Photoanodes for Improved Solar Water Splitting. *J. Mater. Chem. A* **2016**, *4*, 2919−2926.
(36) Vincent, G.; Bois, D.; Pinard, P. Conductance and Capacitance Studies in Gap Schottky Barriers. *J. Appl. Phys.* **1975**, *46*, 5173−5178.
(37) Toma, F. M.; Cooper, J. K.; Kunzelmann, V.; McDowell, M. T.; Yu, J.; Larson, D. M.; Borys, N. J.; Abelyan, C.; Beeman, J. W.; Yu, K. M.; et al. Mechanistic Insights into Chemical and Photochemical Transformations of Bismuth Vanadate Photoanodes. *Nat. Commun.* **2016**, *7*, 12012.
(38) Leelavathi, A.; Mukherjee, B.; Nethravathi, C.; kundu, S.; Dhivya, M.; Ravishankar, N.; Madras, G. Highly Photoactive Heterostructures of PbO Quantum Dots on TiO_2. *RSC Adv.* **2013**, *3*, 20970−20977.
(39) Gnanam, S.; Rajendran, V. Optical Properties of Capping Agents Mediated Lead Oxide Nanoparticles Via Facile Hydrothermal Process. *Int. J. Nanomater. Biostructures* **2011**, *1*, 12−16.
(40) Chen, S.; Truax, L. A.; Sommers, J. M. Alkanethiolate-Protected PbS Nanoclusters: Synthesis, Spectroscopic and Electrochemical Studies. *Chem. Mater.* **2000**, *12*, 3864−3870.
(41) Sun, L.; Bao, L.; Hyun, B.-R.; Bartnik, A. C.; Zhong, Y.-W.; Reed, J. C.; Pang, D.-W.; Abruna, H. D.; Malliaras, G. G.; Wise, F. W. Electrogenerated Chemiluminescence from PbS Quantum Dots. *Nano Lett.* **2009**, *9*, 789−793.
(42) Ogawa, S.; Hu, K.; Fan, F.-R. F.; Bard, A. J. Photoelectrochemistry of Films of Quantum Size Lead Sulfide Particles Incorporated in Self-Assembled Monolayers on Gold. *J. Phys. Chem. B* **1997**, *101*, 5707−5711.
(43) Li, R.; Zhang, F.; Wang, D.; Yang, J.; Li, M.; Zhu, J.; Zhou, X.; Han, H.; Li, C. Spatial Separation of Photogenerated Electrons and Holes among {010} and {110} Crystal Facets of $BiVO_4$. *Nat. Commun.* **2013**, *4*, 1432.
(44) Mizrahi, A.; Wignacourt, J.-P.; Drache, M.; Conflant, P. New Phases in the Binary System PbO−$BiVO_4$: Pb_2BiVO_6 and Pb_4BiVO_8. *J. Mater. Chem.* **1995**, *5*, 901−904.
(45) Rouff, A. A.; Elzinga, E. J.; Reeder, R. J.; Fisher, N. S. X-Ray Absorption Spectroscopic Evidence for the Formation of Pb(II) Inner-Sphere Adsorption Complexes and Precipitates at the Calcite-Water Interface. *Environ. Sci. Technol.* **2004**, *38*, 1700−1707.

DOI: 10.1021/acsenergylett.6b00728
ACS Energy Lett. 2017, 2, 469−475